

Investigation of the bulk and surface microstructure of bitumen by atomic force microscopy

Blom, Johan; Soenen, Hilde; Katsiki, Antigoni; Van den Brande, Niko; Rahier, Hubert; van den Bergh, Wim

Published in:
Construction and Building Materials

DOI:
[10.1016/j.conbuildmat.2018.05.062](https://doi.org/10.1016/j.conbuildmat.2018.05.062)

Publication date:
2018

License:
CC BY-NC-ND

Document Version:
Accepted author manuscript

[Link to publication](#)

Citation for published version (APA):

Blom, J., Soenen, H., Katsiki, A., Van den Brande, N., Rahier, H., & van den Bergh, W. (2018). Investigation of the bulk and surface microstructure of bitumen by atomic force microscopy. *Construction and Building Materials*, 177, 158-169. <https://doi.org/10.1016/j.conbuildmat.2018.05.062>

Copyright

No part of this publication may be reproduced or transmitted in any form, without the prior written permission of the author(s) or other rights holders to whom publication rights have been transferred, unless permitted by a license attached to the publication (a Creative Commons license or other), or unless exceptions to copyright law apply.

Take down policy

If you believe that this document infringes your copyright or other rights, please contact openaccess@vub.be, with details of the nature of the infringement. We will investigate the claim and if justified, we will take the appropriate steps.

Investigation of the bulk and surface microstructure of bitumen by atomic force microscopy

Johan Blom^{1*}, Hilde Soenen², Antigoni Katsiki³, Niko Van den Brande³, Hubert Rahier³,
Wim van den Bergh¹

¹*Faculty of Applied Engineering, EMIB-research group, University of Antwerp, 171
Groenenborgerlaan, Antwerp, 2020, Belgium*

²*Nynas N.V., 171 Groenenborgerlaan, Antwerp, 2020, Belgium*

³*Physical Chemistry and Polymer Science (FYSC), Vrije Universiteit Brussel (VUB), Pleinlaan 2,
B-1050 Brussels, Belgium*

*e-mail: johan.blom@uantwerpen.be

Keywords: Atomic Force Microscopy (AFM), Bitumen, Bee structures, Fracture surface,

Abstract

Bitumen, the heavy residue of crude oil, can display a rich microscale morphology, including so-called Bee structures. The use of Atomic Force Microscopy (AFM) measurements in literature strongly indicates that the appearance of Bee structures is related to the presence of paraffin wax crystals. Most studies have investigated standard bitumen surfaces when cooling bitumen in an air atmosphere. Only a few investigations have analysed surfaces formed in other media or have analysed fractured surfaces which relate to the bulk morphology. Although considerable research has focussed on identifying Bee structures, less attention has been paid to the Bee structure morphology of different bitumen types and the relations to other binder parameters. The comparison between the micro morphology of the air-oil interface compared to the bulk phase volume has been studied even less.

In this experimental study, five bitumen samples were selected based on differences in their natural wax content. Both the air-cooled surface interface and fractured surfaces were characterised using AFM in tapping mode. All the air-cooled surfaces revealed Bee structures, except the wax-free bitumen, which did not display the presence of any Bee structure. None of the fracture surfaces revealed Bee structures. Reheating a fractured surface of a wax-containing bitumen transformed the morphology into Bee structures.

The experiments demonstrate that Bee structures are present in different binders but display very different shapes and sizes. However: image analysis indicates that the unit cell inside these structures is rather constant and independent of the binder type. This work confirms a relationship between natural wax and Bee structures and it also shows that Bee structures, as such, are a surface phenomenon which is not present in the bulk phase volume of samples.

• Introduction

Bitumen, obtained as the residue from crude oil after distillation, has excellent waterproofing and binding properties and is an important component of our asphalt pavements. Chemically, bitumen consists mainly of hydrocarbons, including saturated and aromatic structures, which can be arranged in many different configurations. In addition, small percentages of sulphur, nitrogen and oxygen, and traces of vanadium, nickel, magnesium, iron and calcium can be present [1]. Although the general elemental composition of bitumen and the type of functional

chemical groups are well established, there are still a lot of uncertainties with regard to the microstructure, ranging from a colloidal system, in which asphaltenes are dispersed in a matrix of maltenes, to an almost single-phased material. And, there is still a large gap in understanding the relations between the chemical, microstructural and mechanical properties [2-4].

The characterisation of surface structures on a nanoscale level became possible with the development of the atomic force microscope (AFM) in 1986 by Binnig et al.[5]. Loeber et al. (1996, 1998) [6,7], one of the first authors showing AFM images of bitumen. These images revealed rippled microstructures represented by yellow and black strips, which were referred to as “Bees” by the author. In these initial studies, Bee structures were concluded to be a structuring of asphaltenes. Further evidence for this conclusion was provided in literature. In 2001, the group of Pauli et al. [8] investigated Bee structures after doping bitumen with extra asphaltenes. An increase in the concentration of asphaltenes could be related to an increase in the density of Bee-shaped microstructures on the bitumen surface. Jäger et al. (2004) [4] observed Bee structures on the surface of asphaltenes, while no such structures could be detected on maltene surfaces. Masson et al. (2006) [9], studied 13 bitumen types, and in this study, no correlation between the AFM morphology and the four components analysis of bitumen into saturates, resins, aromatics and asphaltenes could be indicated.

Depending on the mode of measurement - tapping versus pulsed-force mode - AFM not only provides insight into the surface topography but can also assess differences in stiffness and adhesion properties on a nanoscale level. This technique allowed to relate differences in topography on a bitumen surface to differences in mechanical and adhesive properties [10-16]. Jäger et al. (2004) [4], for example, identified four different material phases at the bitumen-scale with different topography and stiffness properties. In his paper the bitumen surface was cooled during the experiments, using a Peltier element. There was also a long-time delay of 7 days between sample preparation and testing.

Bee structures have also been related to a crystallisation of natural wax and several studies [17, 18] have provided strong evidence for this. For example, the RILEM technical committee 231 on nano bituminous materials, applied AFM at different temperatures for different types of binders and could correlate the changes in the Bee structures to signals in differential scanning calorimetry (DSC) measurements (Das et al. 2013; Fischer et al., 2013a; Soenen et al., 2014) [19- 21]. Moreover, tests demonstrated that a wax-free bitumen did not reveal any type of structure. Bee structures appeared on the surface only after adding commercial waxes to this bitumen. Regarding the mechanism why Bees are formed, Asa Laurell Lyne (2013) made a significant contribution [22]. She proposed a mechanism based on the solid-liquid phase separation and differential contraction of paraffin wax crystals during cooling from the hot liquid state. Because of differences in the elastic modulus of the wax compared to the matrix, this leads to a wrinkling of the surface. The assumption that the rippled surface morphologies are paraffin wax crystals in a strained configuration was also put forward by Pauli et al. (2014) [23]. Fischer & Cernescu (2015) [24] also supported this conclusion.

In addition, many studies also revealed that AFM images are highly dependent on the thermal history, sample preparation and analysis conditions [25-29]. Nahar et al., (2015) [30] illustrated that, in addition to the particular binder type, parameters such as the thickness of the sample, heat treatment temperature and duration, play an important role in the size and shape of the Bee structures. The exposure of bitumen films to other media, such as water, also influences the microstructures, including the topographical and mechanical properties. It was shown that increasing exposure times to water flattens out the difference in surface height [31]. In the work of Hung (2017) [32], samples exposed to water at ambient temperature showed the formation of “nano-bumps”. It was hypothesized that these nano-bumps are absorbing water and seeping up from underneath the Bee structure. The valleys of the Bee structure as well as the interfaces contain material with different mechanical properties from

the surrounding surface.

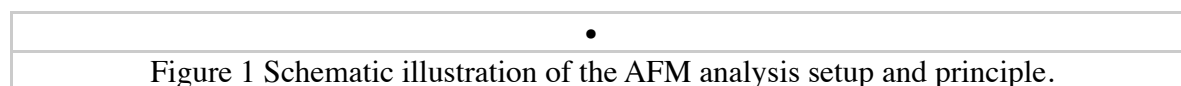
A few studies have investigated the microstructures in the bulk state of the binder. Fischer, Dillingh, and Hermse (2014) [33] and Yue Hou (2017) [34] performed AFM tests on both the surface and the bulk. These experiments showed Bee structures only on the surface. In the bulk phase circular structures were observed, these became more obvious when scanning acoustic microscopy was applied. In this research, the bulk phase was evaluated by means of the fracture surface, which was prepared after freezing (-20°C) the sample followed by a brittle fracture. The AFM measurements were performed at room temperature.

In this study, the AFM technique is applied to a set of bitumens from different origins and differing in the natural wax content. This should enable one to observe the formation of Bee structures and possibly to confirm relations between these bee structures and the presence of natural wax or other binder parameters. Secondly, the same binders are evaluated in the bulk structure by means of preparing fracture surfaces to investigate what type of microstructures can be formed in the bulk phase. Finally, a fractured surface is reheated and evaluated.

- Experimental part
 - Experimental setup

2.1.1 Atomic Force Microscopy (AFM)

Atomic-force microscopy (AFM) is a technique based on the interaction between the sample and a tiny probe, called the cantilever (Fig. 1). [5]



The cantilever holds a sharp tip, which is the actual part that interacts with the sample surface. By scanning a sample surface and plotting how these interactions change in function of the x-y position, an image can be obtained which plots several physical properties such as, e.g., the sample roughness. The basic working principle of AFM is that a sharp tip attached at the end of a cantilever, probes the specimen surface with a laser beam focused at the end of the cantilever reflecting into a photodetector to track the surface topography.

Tapping-Mode AFM, is a high-amplitude dynamic mode where an amplitude modulation feedback is used to image the sample topography [Error! Reference source not found.-39]. The cantilever-tip ensemble is oscillated at a frequency close to its resonance frequency. This oscillation of the cantilever is triggered by the distance between tip and sample surface. During the sample scan the oscillation amplitude is kept at a fixed value. This can be obtained by varying the Z axis, height, using a feedback loop. Catering the Z axis data for each point during scanning results in a high-resolution imaging of surface topography. Although the Tapping-Mode offers advantages when measuring low viscosity samples, other AFM techniques with diverse imaging modes for microscopic characterization of different phases, mechanical properties and other phenomena of various materials exist [45,46].

2.12. AFM instrumental settings

The measurements were performed using the AFM [44] setup available at the Physical Chemistry and Polymer Science (FYSC) the parameters used are presented in Table 1. All AFM scans were performed using tapping mode in air and at room temperature 20 °C. In this case an AC 160 TS silicon cantilever [47] tip is used. This measuring probe is a piece cut from a Si wafer, and a tiny cantilever is formed on it. The back side of the cantilever has a reflective coating to increase the laser signal as well as to protect the bitumen sample from softening by laser exposure. The typical dimensions of the cantilever are 160x40x3.7 μm. Tests were performed using resonance frequency 300 +/- 100kHz, and a typical spring

constant of 26 N.m^{-1} . As mentioned, AFM is based on the interaction between a sample and a tiny probe. In this case, the AFM measuring head can only move in the Z direction. This vertical Z-axis displacement is limited to a travel distance of $15 \mu\text{m}$. The sensor noise is less than 25 nm , with an average deviation in a 0.1 Hz - 1 kHz bandwidth and sensor non-linearity less than 0.05% (max deviation/full travel) at a full scan. The Z height noise is less than 0.06 nm . In order to scan the surface, specimens are placed on a table with an X and Y activator. The travel distance in X & Y is limited to $90 \mu\text{m}$ and controlled by a closed loop. It is position controlled with sensor noise $<0.5 \text{ nm}$ average deviation in a 0.1 Hz - 1 kHz bandwidth and sensor nonlinearity $<0.5\%$ (max deviation/full travel) at full scan [44].

Table 1: General settings of the AFM

Scan size	20	μm
Scan rate	0.80	Hz
Scan angle	0	$^{\circ}$
Scan speed	39.86	$\mu\text{m/s}$
Set point	650.00	mV
Drive amplitude	9.77	mV
Drive frequency	300	Hz

• Materials

2.2.1 Sample selection

Five binders were selected, based on differences in their natural wax content. The wax content was evaluated from the melting enthalpy (H_m), determined by Differential Scanning Calorimetry (DSC). The DSC test consisted of two steps; a cooling scan, from $+140$ to -60 $^{\circ}\text{C}$ followed by a heating scan in the same temperature region, both at a scanning rate of 10 $^{\circ}\text{C/min}$; If there was a melting signal in the heating scan, its enthalpy was determined, by integrating the melting signal. This was achieved by linearly extending the base line observed in the melt. More details on this procedure, together with some examples can be found in the publication by Soenen, H. & Redelius P., [48]. In Table 2 empirical tests results and enthalpy measurements derived from DSC, are shown for the five selected binders. The data illustrate the variation in the melting enthalpies: in this respect, the wax is defined as the material that melts upon heating. Sample D does not contain any natural wax; its melting enthalpy is 0 J/g , larger melting enthalpies (H_m) indicate a higher wax content. The end temperature of the melting region is also indicated in Table 2. For the samples that contain natural wax, this temperature is between 80 and 90 $^{\circ}\text{C}$. In addition, binders were investigated by Fourier Transform Infrared Spectroscopy (FTIR) combined with attenuated total reflection (ATR). The instrument used was a Nicolet IS 10, with a diamond cell (smart-orbit). Sample pre-treatment is very simple, binders are heated until they can be poured onto the ATR crystal, and to obtain a good contact between sample and prism, a small sample press, delivered with the instrument is available. More details can be found in ref [48]. For the five selected binders, only minor differences were observed in the spectra. There was a difference in the band at about 725 cm^{-1} , which is related to a CH_2 rocking band. In some of the binders, B, C and E, this band showed indications of a splitting, as indicated in Fig. 2. In literature, it has, among other things, been suggested that a splitting of this band into two components at 721 cm^{-1} and 731 cm^{-1} arises from interactions between adjacent molecules in the crystalline phase, which results in both an in-phase and an out-of-phase rocking mode [51].

Figure 2: FTIR-ATR spectra of bitumen, with a magnification of the 730-720 cm^{-1} wavenumber region

The binders were also analysed by Western Research Institute (Laramie USA) using their patent-pending automated SAR-AD (Saturates, Aromatics, Resins, Asphaltene Determinator) technique, which is a combined precipitation and chromatographic analysis that separates a sample into solubility fractions. These results are shown in Table 3. In this procedure, the main difference as compared to the standard SARA analysis, is that the asphaltene fraction is separated further and is selectively dissolved with cyclohexane (C_6H_{12}), toluene, and finally, methylene chloride methanol (98:2 v:v) (referred to as the MeOH fraction in Table 2) resulting in three asphaltene fractions. More details on this technique can be found in [49-50]. The data indicate only minor differences between the binders and also show that all the samples have an asphaltene content within expected limits.

Table 2: Properties of the bitumen samples

Sample	Pen at 25 °C		R&B	H_m (J/g)		T_m -end	
A	42	mm/10	51.3	2.8	J/g	81	°C
B	52	mm/10	49	6.8	J/g	84	°C
C	52	mm/10	49.8	6.2	J/g	90	°C
D	64	mm/10	47.7	0	J/g	-	°C
E	67	mm/10	46.8	7.6	J/g	84	°C

Table 3: SAR-AD analysis of the bitumen samples

Sample	Saturates		Aromatics		Resins		Asphaltenes		Asphaltene sub fractions
							C_6H_{12}	Toluene	MeOH
A	12.9	62.7	14.1	10.4	2	8.2	0.2		
B	18.9	57.7	8	15.4	0.5	14.2	0.7		
C	18.3	55	11	15.7	1.4	14.1	0.2		
D	22.5	49.5	15	13	1.7	11	0.3		
E	23.2	55.9	6.8	14	0.5	12.9	0.6		

2.2.2. Sample preparation for AFM

- *Air-cooled surfaces.*

To prepare the air-cooled surfaces, the bitumen samples were first heated in an oven to 160°C (30 min). Afterwards, approximately 20 mg was applied to the AFM sample substrate, an aluminium sample disk with a diameter of 12 mm. The specimens were subsequently reheated on a hot plate of 100°C for 30 seconds to create a thin flat film, Figure 3A. After preparation, to avoid any particle pick-up, the specimens were stored inside a closed box at room temperature, for a maximum of 24 hours before testing in the AFM.

- *Fracture surfaces*

A slightly different sample preparation was used to prepare fracture surfaces: in this case, bitumen was also heated in an oven, but the sample drops were placed on a glass plate and immediately covered by a second glass plate, Figure 3B. Before fracturing, the specimens were stored at -22°C for 2h. Pulling the two glass plates apart induced a brittle fracture within the bitumen phase, which produced flat fracture surfaces as shown in Figure 3C. After fracturing, the specimens were stored between 5-30 minutes at room temperature before

testing them.

• <i>Air-cooled surface</i>	• <i>Pre – Fractured surface</i>	• <i>Fracture surface</i>
Figure 3: Bitumen sample preparation		

• Results & Discussion

The results of the AFM measurements are presented in three sections. First, images of bitumen air-cooled surfaces are shown. In a second section, AFM images on fractured surfaces are presented and the last part includes images of a reheated fractured surface.

• 3.1 Air-cooled surfaces.

The images; height, phase and amplitude, from an AFM scans of the air-cooled surface of bitumen sample A are shown in Figure 4.

<i>Sample A</i>		
<i>Height</i>	<i>Phase</i>	<i>Amplitude</i>
Figure 4: Images obtained by AFM of an air-cooled surface of bitumen A		

These images clearly show Bee structures, which can be distinguished as a regular topographic pattern of higher and lower levels, Figure 5. Sample A is characterized by a high amount of randomly distributed single Bee structures. The phase image shows a distinct spherical phase around each of the Bees, which is in turn surrounded by a darker matrix. This is also visible in the amplitude and height image, but not so clear, which indicates that this surrounding phase could be more related to hardness differences as compared to a topographic effect [9],[53].

Figure 5: Dimensions and characterization of a Bee structure.

The Bee unit cell, its total length (L) and the distribution, were determined by image processing. In this case, an open source Java image processing program, J image, developed by NIH Image [51] was used. By calibrating the image obtained from the AFM height scan, Figure 5, an average cell length (L) of $1.4 \mu\text{m}$ (SD. 0.1) was derived. For sample A, each Bee structure contains on average three-unit cells, and a “unit” measures $0.28 \mu\text{m}$ (SD. 0.02). This results in an average wave length (λ) of $0.560 \mu\text{m}$. According to Jäger et Al [4], the distance λ in the Bee structure for various bitumen types was around $0.550 \mu\text{m}$, which is comparable with the results in this study.

Image processing was also used to count the unit cells, and to evaluate the surface distribution. The results of the surface analysis are presented in Figure 6. It is clear that the phase surrounding the Bee structure is not counted in this analysis. In case of sample A, 129-unit cells were counted. Compared to the total observed surface ($20 \times 20 \mu\text{m}$), the until cells cover 2.48 %. This type of image analysis was applied to all the images, keeping filter parameters identical. Image analysis data are presented in Table 4. In all cases the five areas of $20 \times 20 \mu\text{m}$ were examined.

Figure 6: Image (height) obtained by AFM and processed image enabling to count the unit cells.
--

The AFM scans of the air-cooled surface of bitumen B, figure 7, show a different distribution

compared to the previous measurement performed on bitumen A. In this case, the number of Bees is reduced but their size, in particularly the transversal width, has increased, clearly shown in figure 6 B. In some cases, it also seems that bees with different orientations overlap and touch each other, such an example is marked in figure 7, in the height image.

Height	Phase	Amplitude
<i>Figure 7: Images obtained by AFM of an air-cooled surface of bitumen B</i>		

In this sample, the average length of the Bee structure was $4.1 \mu\text{m}$ (SD. 1.0), which is larger as compared to the sizes in bitumen A. The average unit cell size of this sample is $0.29 \mu\text{m}$ (SD. 0.05) and is comparable to the one found for sample A ($0.28 \mu\text{m}$). Note that the standard deviation has increased slightly, indicating a larger variation of the unit cells. For binder B, cell counting resulted in 89-unit cells, covering 2.55% of the observed surface.

For sample C, the AFM images are represented in Figure 8. The images show a very different distribution of the Bee structures, as compared to the previous two samples. Also note the difference in scales between this and previous figures. In this case the unit cells are connected into long chains, with an average length exceeding $30 \mu\text{m}$, and there is a clear overlap of chains with different orientations. Nevertheless, the average unit cell size is comparable to the pervious bitumen samples, $0.29 \mu\text{m}$ (SD. 0.08). After the filtering process, an average of 36-unit cells are counted, covering by approximation 1.77% of the surface. However, in this case the quantitative analysis should be treated with care. First of all, due to the complex structure, illustrated by a profile scan in Figure 8, evaluating the number of cell units and the coverage become challenging. And, as the structures are not homogeneously distributed inside the figure, the quantitative measure of coverage is also less accurate. In Table 4 the measure of coverage is an average value (16 measurement $20 \times 20 \mu\text{m}$) of the larger figure ($80 \mu\text{m} \times 80 \mu\text{m}$)., figure 8.

Height	Phase
<i>Figure 8: Sample "C" Length of the "Bee" structure</i>	

For sample D, the enthalpy measurement as indicated in Table 2, shows that this sample does not have any natural wax. This is also reflected in the AFM images, where no Bee structures nor any other structure could be detected, Figure 9.

Sample C		
Height	Phase	Amplitude
Sample D		
Height	Phase	Amplitude
Sample E		
Height	Phase	Amplitude
<i>Figure 9: Image obtained by AFM of an air-cooled surface of bitumen C, D and E.</i>		

In contrast to bitumen D, sample E contains a large amount of wax, resulting in the formation of Bee structures in the surface, figure 9. When looking to the images, Bee structures clearly overlap and seem to form a kind of star structure, with a resemblance to the spherulitic growth of polymer crystals [54]. For the average unit cell size, a value of $0.29 \mu\text{m}$ (SD. 0.11) is

obtained, while the number of cells in this sample is 98. The Bee coverage is by approximation 3.24%. Note the large standard deviation in the unit cell size.

Table 4: overview of image processing data

Samp le	Size unit cell		SD	Unit Cells	SD	Cover age		SD	H _m	
A	0.28	μm	0.02	129	7.71	2.48	%	0.25	2.8	J/g
B	0.29	μm	0.05	89.4	12.78	2.55	%	0.41	6.8	J/g
C	0.29	μm	0.08	35.69	14.29	1.77	%	0.78	6.2	J/g
D	/	μm		0	0	0	%	0	0	J/g
E	0.29	μm	0.11	98	14	3.24	%	1.38	7.6	J/g

The measurement of the unit cell size shows that this parameter is rather constant for all the samples, as far as they display Bee structures, even for samples with very different Bee morphologies. According to literature, this is an argument that the Bee pattern is due to a crystallization of the same specific structure in all the samples [18]. The observation of a constant unit cell could also point to a wrinkling driven mechanism [22], if we assume that the thickness of the structures is similar.

The unit cell counts and unit cell coverages are different for all the investigated samples. Regarding the melting enthalpy, it is clear that sample D which has no melting substances also has no Bee structures. This has already been reported in the literature and is reconfirmed. In addition, when comparing the unit cell coverage to the melting enthalpy, there is a trend that a larger melting enthalpy results also in a larger cell coverage. However, the trend is not very accurate: the linear coefficient of determination (R^2) is only 0.67. This may have different reasons; the cell coverage is only based on a surface measurement, with no information on the bulk sample, and as mentioned before for some samples the cell coverage is less accurate, due to the complex and overlapping structures, and the non-homogeneous distribution of the Bees in the images. In addition, the thermal histories of the samples investigated in AFM and in DSC were not exactly the same. In DSC, the melting enthalpy was measured directly after a cooling scan, while in AFM samples had been at room temperature for a period up to 24 hours.

When comparing the CH₂ vibrational rocking bands analysed by FT-IR to the Bee structures, one can observe that samples with double bands at 730 cm⁻¹ and at 721 cm⁻¹, tend to have more overlapping Bee structures. If we assume that the occurrence of two bands is related to interactions between adjacent molecules in the crystalline phase, this would also point to a crystallization of waxy compounds. As was mentioned in the introduction, some researchers have observed Bees only in the asphaltene fraction of bitumen or have observed an increase in the Bee structure coverage when adding asphaltenes to bitumen. This observation is also consistent with a wax crystallization, since the determination of the percentage of asphaltenes, as well as its separation from bitumen, is based on solubility properties. And, as has been reported in literature [55], also linear aliphatic chains become insoluble in n-heptane from a certain chain length and temperature. Consequently, they will appear in the asphaltene fraction, although they do not have the typical chemical structure which is associated to asphaltenes.

• 3.2 Fracture surface (Bulk)

In this part, the images obtained on fracture surfaces are discussed. For all the samples, the

fracture surfaces do not display the typical Bee structures, as they are observed on air-cooled surfaces, figure 10. Nevertheless, in some cases ring like structures are observed, especially when specimens are measured directly after fracturing at a low temperature (-22°C). These ring like structures were more pronounced in the phase images.

<i>Sample A</i>		
<i>Height</i>	<i>Phase</i>	<i>Amplitude</i>
<i>Sample B</i>		
<i>Height</i>	<i>Phase</i>	<i>Amplitude</i>
<i>Sample C</i>		
<i>Height</i>	<i>Phase</i>	<i>Amplitude</i>
<i>Sample D</i>		
<i>Height</i>	<i>Phase</i>	<i>Amplitude</i>
<i>Sample E</i>		
<i>Height</i>	<i>Phase</i>	<i>Amplitude</i>

Figure 10: Image obtained by AFM scan of fracture surface bitumen samples

An example is shown in Figure 11 for bitumen B; in one case, the upper three images, the AFM test was made relatively quickly after fracturing the sample (about 5 minutes), while for the images in the lower row the AFM was taken about 20 minutes after fracturing the sample. Although circular structures on fracture surfaces have been observed before [32,33], it is not fully clear where these structures come from, and the authors are suspecting an artefact, coming from the condensation of water that may have interfered with the surface as these samples were frozen and then fractured. Even when the water is removed before testing there could still be an imprint on the bitumen surface, as was indicated by studies investigating the effects of water in AFM [32]. Further investigations with regard to possible water condensation effects needs to be performed.

<i>Sample B</i>		
<i>Height</i>	<i>Phase</i>	<i>Amplitude</i>
<i>Sample B*)</i>		
<i>Height</i>	<i>Phase</i>	<i>Amplitude</i>

Figure 11: Image obtained by AFM of fracture surfaces of bitumen B; upper three images, the AFM test is performed about 5 minutes after fracturing the binders, lower three images, the AFM test is performed about 20 minutes after fracturing the sample.

3.3 Fracture surface (Bulk) reheated

Finally, some of the fracture surfaces were reheated in an oven and reinvestigated in the AFM at 20°C. The reheated images are shown for sample A, in figure 12. These images clearly show that the Bee structures have re appeared and image processing indicates an average unit cell of 28 μm and counts 127-unit cells, very similar to what was observed in the original air-cooled sample. Upon reheating a fracture surface, the Bees appear again, and this confirms that the components that build up the bees are present in the bulk. At this stage, it was not possible to check if the reappearance of the Bees is related to the position of the circular structures on the surface. It should also be noted that this sample was tested almost directly after reheating and not 20-24 hours after the oven treatment as was done for the first set of air-

cooled samples.

Height	Phase	Amplitude

Figure 12: AFM images of a reheated, fractured surface of bitumen A

• Conclusion

The AFM measurements on air-cooled bitumen surfaces show a wide range of Bee structure configurations. Binders from different origins display very different shapes and sizes of Bee structures. Small, isolated Bees have been observed, as well as very large, strongly overlapping structures. The wax content as determined by DSC, did not relate to the Bees morphology. A similar melting enthalpy can still result in very different Bee morphologies. But bitumen with a larger melting enthalpy in DSC measurements tend to have an increased coverage with Bee structures. In samples where the appearance of the CH₂ rocking vibration, tested by FTIR-ATR, showed band splitting, in those cases it was observed that also the Bee structures showed overlapping morphologies. Although the Bee structures from different binders display different shapes and sizes, the unit cell, inside the structure is almost constant (0.29 μm) and independent of the binder type and its wax content.

A simple test method to create flat fracture surfaces is presented. Fracture surfaces did not reveal any Bee structures, this indicates that Bees are only formed on a surface, formed when the mobility is high or the viscosity is low, in this case only surfaces in contact with air were investigated. However, on some the fractured surfaces circular shapes could be observed, which were more pronounced in the phase images. At this moment, the possibility of having artefacts resulting from a possible condensation of water in the fractured tests is still under investigation.

Reheating a fracture surface of a wax containing bitumen in an oven up to liquidity transformed the morphology into bee structures. This indicates that wax containing material is still present in the bitumen bulk phase after fracturing and that upon reheating it can transform quickly and form Bee structures on the surface.

At this moment, all the observations point into a direction that Bees are only formed on (air)-cooled surfaces, whether this surface needs to be cooled in air or whether any other medium would also induce these structures is still open. And at this moment, the observations are consistent with the explanation that natural wax is responsible for the Bee structures. In this respect, for the two trends that were observed, one between bee coverage and wax content and one between Bee overlap and FTIR-ATR absorptions, these are at this moment only based on the 5 binders investigated.

References

- Xiaohu Lu, Peter Sjövall, Hilde Soenen, (2017), Structural and chemical analysis of bitumen using time-of-flight secondary ion mass spectrometry (TOF-SIMS), In Fuel, Volume 199, , ISSN 0016-2361, pages 206-218.

- Bearsley S., Forbes A., Haverkamp R.G., (2004), Direct observation of the asphaltene structure in paving-grade bitumen using confocal laser-scanning microscopy, *Journal of Microscopy*, Vol. 215, Pt 2 August 2004, pages 149 –155.
- Lesueur D., (2009), Evidence of the Colloidal Structure of Bitumen, Published in *Proc. ISAP International Workshop on Chemo-Mechanics of Bituminous Materials*, N. Kringos Ed. – Delft Univ., pages.39-48.
- Jäger A., Lackner R., Eisenmenger-Sittner C., & Blab R. (2004). Identification of four material phases in bitumen by atomic force microscopy. *Road Materials and Pavement Design*, 5(suppl.), pages 9–24.
- Binnig G., Quate C. F., & Gerber C. (1986). Atomic force microscope. *Physical Review Letters*, 56(9), pages 930–933.
- Loeber L., Sutton O., Morel J., Valleton J.-M., & Muller G. (1996). New direct observations of asphalts and asphalt binders by scanning electron microscopy and atomic force microscopy. *Journal of Microscopy*, 182(1), pages 32–39.
- Loeber L. Muller, G. Morel, J. & Sutton, O. (1998). Bitumen in colloid science: A chemical, structural and rheological approach. *Fuel*, 77(13), pages 1443–1450.
- Pauli A. T., Branthaver J. F., Robertson R. E. Grimes, W. & Eggleston C. M. (2001). Atomic force microscopy investigation of SHRP asphalts. *ACS Division of Fuel Chemistry*, 46(2), pages 104–110.
- Masson J.-F., Leblond V., Margeson J. (2006). Bitumen morphologies by phase-detection atomic force microscopy. *Journal of Microscopy*, 221(1), pages 17–29.
- Leite F., De Oliveira R.,Albuquerque D.,Cruz T.,Yamaji F., Bellitto V., (2012). Measurement of the Nanoscale Roughness by Atomic Force Microscopy: Basic Principles and Applications, Book: *Atomic Force Microscopy*, Ch. 7, <https://doi.org/10.5772/37583>, DO - 10.5772/37583, InTech, Rijeka., pages 147-174.
- Burnham, N.A.; Colton, R.J., (1989) Measuring the nano mechanical properties and surface forces of materials using an atomic force microscope, *Journal of Vacuum Science & Technology A: Vacuum, Surfaces, and Films* 7, 2906; <https://doi.org/10.1116/1.576168>, 2906–2913.
- Jagtap, R.N.; Ambre, A.H.,(2006), Overview literature on atomic force microscopy (AFM): Basics and its important applications for polymer characterization., *Indian Journal of Engineering & Material Sciences*, Vol.13, CSIR, <http://hdl.handle.net/123456789/7570>, ISSN: 0975-1017 (Online); 0971-4588 (Print), pages 368-384.
- Yongho S and Wonho J,(2007), Atomic force microscopy and spectroscopy, Published 17 December 2007 • 2008 IOP Publishing Ltd , *Reports on Progress in Physics*, Volume 71, Number 1.
- Gavara N. A., (2017), Beginner's guide to atomic force microscopy probing for cell mechanics. ,Toca-Herrera JL, ed. *Microscopy Research and Technique*,80(1):. doi: 10.1002/jemt.22776, pages 75-84
- Sikora A., (2016), Andrzej Sikora. Quantitative Normal Force Measurements by Means of Atomic Force Microscopy Towards the Accurate and Easy Spring Constant Determination. *Nanoscience and Nanometrology*. Vol. 2, No. 1, 2016, doi: 10.11648/j.nsnm.20160201.12 , pages. 8-29.
- Fischer, H., Stadler, H., & Erina, N. (2013b). Quantitative temperature-depending mapping of mechanical properties of bitumen at the nanoscale using the AFM operated with Peak Force Tapping TM mode: Quantitative mapping of mechanics of bitumen. *Journal of Microscopy*, 250(3), pages 210–217.
- Pauli, A.T.; Grimes, R.W.; Beemer, A.G.; Turner, T.F.; Branthaver, J.F, (2011), Morphology of asphalts, asphalt fractions and model wax-doped asphalts studied by atomic force microscopy, *International Journal of Pavement Engineering*, vol 12, nr 4,<https://doi.org/10.1080/10298436.2011.575942>, pages 291-309.

- Pahlavan F., Mousavi M., Hung A., Fini E. H. (2016), Investigating molecular interactions and surface morphology of wax-doped asphaltenes, *Journal of Phys. Chem. Chem. Phys.*, 2016, volume: 18, issue: 13, p.: 8840–8854, publisher: The Royal Society of Chemistry, doi: 10.1039/C5CP07180A.
- Das, P. K., Kringos, N., Wallqvist, V., & Birgisson, B. (2013). Micro-mechanical investigation of phase separation in bitumen by combining atomic force microscopy with differential scanning calorimetry results. *Road Materials and Pavement Design*, 14(suppl.), doi: 10.1080/14680629.2013.774744, pages 25–37.
- Fischer, H., Poulikakos, L. D., Planche, J.-P., Das, P., & Grenfell, J. (2013a). Challenges while performing AFM on bitumen. In N. Kringos, B. Birgisson, D. Frost & L. Wang (Eds.), *Multi-scale modeling and characterization of infrastructure materials* Dordrecht, the Netherlands: Springer, pages 89–98.
- Soenen, H., Besamusca, J., Fischer, H. R., Poulikakos, L. D., Planche, J.-P., Das, P. K., ... Chailleux, E. (2014). Laboratory investigation of bitumen based on round robin DSC and AFM tests. *Materials and Structures*, 47(7), doi: 10.1617/s11527-013-0123-4, pages 1205–1220.
- Lyne, Å. L., Wallqvist, V., Rutland, M. W., Claesson, P., & Birgisson, B. (2013b). Surface wrinkling: The phenomenon causing bees in bitumen. *Journal of Materials Science*, 48(20), doi: 10.1007/s10853-013-7505-4, pages 6970–6976.
- Pauli, T., Grimes, W., Cookman, A., & Huang, S.-C. (2014). Adherence energy of asphalt thin films measured by force-displacement atomic force microscopy. *Journal of Materials in Civil Engineering*, 26(12), 04014089. doi: 10.1061/(ASCE)MT.1943-5533.0001003
- Fischer H.R., Cernescu A., (2015), Relation of chemical composition to asphalt microstructure - Details and properties of micro-structures in bitumen as seen by thermal and friction force microscopy and by scanning near-field optical microscopy., *Fuel*, 153, Elsevier, issn: 0016-2361, <http://www.sciencedirect.com/science/article/pii/S0016236115003397>, pages 628–633.
- Menapace, I., Masad, E., Bhasin, A., & Little, D. (2015). Microstructural properties of warm mix asphalt before and after laboratory-simulated long-term ageing. *Road Materials and Pavement Design*, 16(suppl.), doi: 10.1080/14680629.2015.1029692, pages 2–20.
- Dos Santos, S., Partl, M. N., & Poulikakos, L. D. (2014). Newly observed effects of water on the micro-structures of bitumen surface. *Construction and Building Materials*, 71, doi: 10.1016/j.conbuildmat.2014.08.076, pages 618–627.
- Menapace, I., Masad, E., Little, D., Kassem, E. & Bhasin, A., (2014) Microstructural, chemical and thermal analyses of warm mix asphalt, sustainability, eco-efficiency and conservation in transportation infrastructure asset management, ed. by Losa & Papagiannakis. Taylor & Francis Group, London, pages 157–168
- Nahar, S.N., Schmets, A.J.M., Scarpas, A., Schitter, G. (2013) Temperature and thermal history dependence of the microstructure in bituminous materials, *European Polymer Journal*, vol 48, nr 8, issn: 0014-305, doi: org/10.1016/j.eurpolymj.2013.03.027, <http://www.sciencedirect.com/science/article/pii/S0014305713001596>, pages 1964–1974.
- Fischer, H.R. , Dillingh, E.C., Hermse, C.G.M. (2014a) On the microstructure of bituminous binders. *Road Materials and Pavement Design*, Taylor & Francis; DOI: 10.1080/14680629.2013.837838, <https://doi.org/10.1080/14680629.2013.837838>, pages 1–15.
- Nahar, S.N., Schmets, A.J.M., Kasbergen, C., Schitter, G. & Scarpas, A. (2015) Self-Healing of Bituminous Materials by Damage Reversal at the Microstructural Scale, THE 94th Annual Meeting of the Transportation Research Board, January 11–15,

Washington, DC.

- dos Santos S, Partl M. N., Poulikakos L.D.,(2014), Newly observed effects of water on the microstructures of bitumen surface, *Construction and Building Materials*, Volume 71, 30 November 2014, ISSN 0950-0618., <http://dx.doi.org/10.1016/j.conbuildmat.2014.08.076>, pages 618-627.
- Hung A.M., Goodwin A., Fini E.H.,(2017), Effects of water exposure on bitumen surface microstructure *Construction and Building Materials*, Volume 135, 15 March 2017
- Fischer H.R., Dillingh E.C., (2014), On the investigation of the bulk microstructure of bitumen - Introducing two new techniques, *Fuel* 118, doi:10.1016/j.fuel.2013.11.008.
- Hou Y, Wang L, Wang D, Guo M, Liu P, Yu J., (2017), Characterization of Bitumen Micro-Mechanical Behaviors Using AFM, *Phase Dynamics Theory and MD Simulation*. Abdel Wahab M, ed. *Materials*. 2017;10(2):208. doi:10.3390/ma10020208.
- Voigtländer B., (2015), Amplitude Modulation (AM) Mode in Dynamic Atomic Force Microscopy. In: *Scanning Probe Microscopy. NanoScience and Technology*. Springer, Berlin, Heidelberg, DOI 10.1007/978-3-662-45240-0_14, ISBN 978-3-662-45239-4.
- Bruker Nano Surfaces, Fundamentals of Contact Mode and Tapping Mode Atomic Force Microscopy, May 18 2012, <https://www.azonano.com/article.aspx?ArticleID=3010>, accessed on April 2018.
- Burnham NA, Colton RJ., (1989), Measuring the nanomechanical properties and surface forces of materials using an atomic force microscope, *Journal of Vacuum Science & Technology A: Vacuum, Surfaces, and Films* A7, 2906 -13, <https://doi.org/10.1116/1.576168>.
- Burnham NA, Dominguez DD, Mowery RL, Colton RJ.,(1990), Probing the surface forces of monolayer films with an atomic-force microscope. *Phys Rev Lett*, vol: 64, issue 16, <https://link.aps.org/doi/10.1103/PhysRevLett.64.1931>, pages 1931-1934.
- Butt H-J, Cappella B, Kappl M., (2005), Force measurements with the atomic force microscope: technique, interpretation and applications, *Surface Science Reports* 59 (2005) 1–152, doi:10.1016/j.surfrep.2005.08.003,
- Robert A. Wilson and Heather A. Bullen, *Introduction to Scanning Probe Microscopy (SPM), Basic Theory Atomic Force Microscopy (AFM)*, Department of Chemistry, Northern Kentucky University, Highland Heights, KY 41099, <http://asdlb.org/onlineArticles/ecourseware/Bullen/SPMTheory.htm>, accessed on April 2018.
- <http://www.vub.ac.be/MACH/FYSC/equipment/atomic-force-microscopy>, accessed on April 2018.
- <http://www.nanophys.kth.se/nanophys/facilities/nfl/afm/fast-scan/bruker-help/Content/TappingMode%20AFM/TappingMode%20AFM.htm>, accessed on April 2018.
- http://afmhhelp.com/index.php?option=com_content&view=article&id=84:what-is-phase-imaging , accessed on April 2018.
- <https://www.asylumresearch.com/Products/Mfp3DSA/Mfp3DSAProduct.shtml#Specifications>, accessed on April 2018.
- Miller EJ, Trewby W, Farokh Payam A, Piantanida L, Cafolla C, Voitchovsky K., (2016), Sub-nanometer Resolution Imaging with Amplitude-modulation Atomic Force Microscopy in Liquid. *Journal of Visualized Experiments*, J. Vis. Exp. (118), e54924, doi:10.3791/54924 ,10 pages.
- Gaczynska M, Osmulski P.A., (2008), AFM of biological complexes: what can we learn? *Current opinion in colloid & interface science*,13, 5, doi: 10.1016/j.cocis.2008.01.004,351-367.
- http://probe.olympus-global.com/en/product/omcl_ac160ts_r3/, accessed on April 2018.

- Soenen, H. & Redelius, P., (2014), The effect of aromatic interactions on the elasticity of bituminous binders, *Rheol Acta* 53 (9): <http://dx.doi.org/10.1007/s00397-014-0792-0>, pages 741–754
- Schabron J. F., Rovani J F, Sanderson M., Loveridge J. L., Nyadong L., McKenna A. M., Marshall A. G., (2012), Waxphaltene Determinator Method for Automated Precipitation and Redissolution of Wax and Asphaltene Components, *Energy & Fuels* 2012 26 (4), DOI: 10.1021/ef300184s, pages 2256-2268.
- Boysen R. B., Schabron J.F.,(2013),The Automated Asphaltene Determinator Coupled with Saturates, Aromatics, and Resins Separation for Petroleum Residua Characterization, *Energy & Fuels* 2013 27 (8), DOI: 10.1021/ef400952b, pages 4654-4661.
- Krimm S.,Liang C. Y., Sutherland G. B. B. M., (1956), Infrared Spectra of High Polymers. II. Polyethylene." *The Journal of Chemical Physics* 25(3): <http://hdl.handle.net/2027.42/70535>, pages 549-562.
- <https://imagej.nih.gov/ij/>, accessed on April 2018.
- Nahar S., Dillingh B., Erkens S., Schmets A., Fischer H., Scarpas T., (2013), Is Atomic Force Microscopy suited as Tool for fast Screening of Bituminous Materials? An Inter-laboratory Comparison Study, Conference Paper · January 2013, <http://www.asfaltblj.nl/media/1472/2012september-27-atomic-force-microscopy-bert-dillingh.pdf>, accesed on April 2018.
- Hobbs J.K., Farrance O. E., Kailas L., (2009), How atomic force microscopy has contributed to our understanding of polymer crystallization, In *Polymer*, Volume 50, Issue 18, 2009, , ISSN 0032-3861, <https://doi.org/10.1016/j.polymer.2009.06.021>,pages 4281-4292.
- Lu X., Kalman B., Redelius P. (2008) A new test method for determination of wax content in crude oils, residues and bitumens, *Fuel* 87, <https://doi.org/10.1016/j.fuel.2007.08.019>, pages 1543–1551